ELSEVIER

Nuclear Instruments and Methods in Physics Research A 377 (1996) 340–345

NUCLEAR INSTRUMENTS & METHODS IN PHYSICS RESEARCH Section A

Performance of the pn-CCD X-ray detector system designed for the XMM satellite mission ☆

H. Soltau[a,*,1], P. Holl[a,1], J. Kemmer[a], S. Krisch[a,1], C. v. Zanthier[a,b,1], D. Hauff[b,1], R. Richter[b,1], H. Bräuninger[c], R. Hartmann[c,1], G. Hartner[c], N. Krause[c,1], N. Meidinger[c,1], E. Pfeffermann[c], C. Reppin[c], G. Schwaab[c,1], L. Strüder[c,1], J. Trümper[c], E. Kendziorra[d], J. Krämer[d]

[a] *KETEK GmbH, Am Isarbach 30, D-85764 Oberschleißheim, Germany*
[b] *Max-Planck-Institut für Physik, Föhringerring 6, D-80805 München, Germany*
[c] *Max-Planck-Institut für extraterrestrische Physik, Giessenbachstraße, D-85740 Garching, Germany*
[d] *Astronomisches Institut der Universität Tübingen, Waldhauserstr.64, D-72046 Tübingen, Germany*

Abstract

The pn-CCD detector system is designed as a focal plane instrument for the European Photon Imaging Camera (EPIC) on the X-ray Multi Mirror mission (XMM) of the European Space Agency. This satellite will be launched by the end of this century. The sensitive area of the detector consists of a $6 \times 6\,cm^2$ array of 12 pn-CCDs monolithically integrated on a single silicon wafer. The detector has been optimized for high-resolution X-ray spectroscopy between 100 eV and 15 keV with simultaneous good quantum efficiency for the investigation of faint objects. A fast readout achieves excellent time resolution for the observation of pulsed X-ray sources.

The relevant performance parameters reflecting the state of the detector development are presented. Energy resolution reaches the theoretical limits given by the Fano noise. Due to a thin entrance window and full depletion of the device the quantum efficiency is better than 80% over a wide energy range. Evidence for radiation hardness and background rejection capability will also be provided.

1. Introduction

The pn-CCD detector system is designed for the X-ray Multi Mirror satellite mission (XMM), which is planned to be launched in 1999. The mission is dedicated to high resolution spectroscopy and imaging of X-ray emitting objects. With its large collecting area (equivalent to $4000\,cm^2$ for 5 keV photons e.g.) the satellite's Wolter telescope allows to study even faint objects (minimal flux $\approx 10^{-15}\,erg\,cm^{-2}\,s^{-1}$).

Accordingly, the requirements for the X-ray detection system include besides good spectroscopic behaviour a high quantum efficiency and a low disturbance level, i.e. high signal to noise ratio and efficient background rejection. Furthermore, due to the projected mission duration of 10 years, long term stability, radiation hardness and independence of supply sources are mandatory.

This research is funded by DARA under contract (50-OX-90020/XMM-EPIC).

* Corresponding author. Tel. +49 89 83940043, fax +49 89 83940011.

Postal address: MPI Halbleiterlabor, Paul-Gerhardt-AUee 42, D-81245 München, Germany.

By the choice of pn-CCDs for the focal plane instrumentation all this criteria can be matched. Their basic concept and primary results have already been published [1,2]. A short overview will be repeated in Section 2. Section 3 will present actual performance parameters, which reflect recent improvements in the design and fabrication of the detectors. We will conclude with a summary of the present development status and an outlook to future activities.

2. Basic concept

Fig. 1 shows a view of the focal plane instrumentation. The sensitive area consists of a $6 \times 6\,cm^2$ array of 12 pn-CCDs monolithically fabricated on a 4 inch silicon wafer. Each CCD unit is 200 pixels deep and 64 pixels wide.

The pn-CCD is a fully depleted radiation detector, which is sensitive over its whole thickness of 280 μm. A schematic cross section through the pn-CCD along the transfer region is shown in Fig. 2. Illumination takes place from the unstructured side through a thin entrance window.

PII S0168-9002(96)00029-0

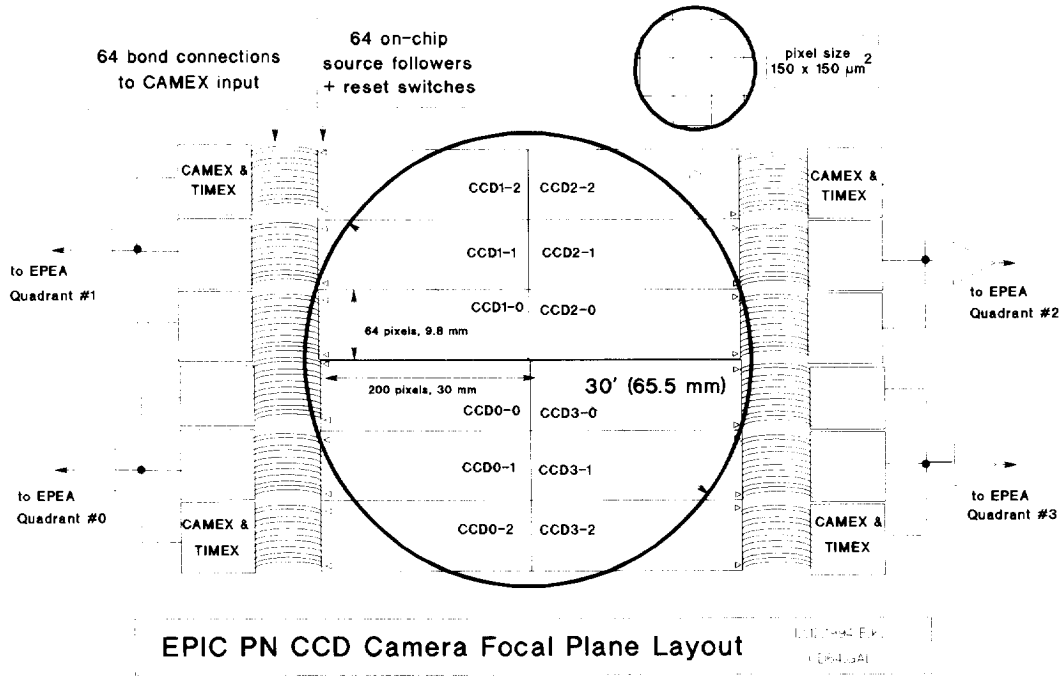

Fig. 1. The pn-CCD focal plane as planned for XMM.

The signal electrons generated in the silicon are drifting very fast (within 1 ns) as a small cloud into the transfer channel, which is located 12 μm below the surface. During the signal integration phase they are stored in pixels represented by local potential minima. Three electrically active registers realized by p^+ implanted strips and a channel stop structure formed by deep implants confine a pixel in the coordinates parallel and orthogonal to the transfer direction respectively.

During readout an appropriate voltage pulse sequence applied to the registers shifts the electrons to the anodes.

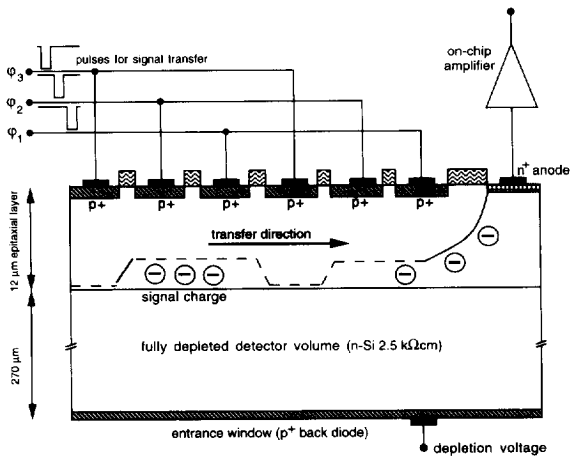

Fig. 2. A schematic cross section through the pn-CCD along a transfer channel.

As a first amplifying stage an n-channel JFET is integrated on the CCD chip close to each anode and significantly reduces stray capacitance and noise.

In the next stage the 64 signals of each row are fed in parallel to the CAMEX64B chip [3] for further amplification, shaping and multiplexing. The CAMEX output is digitized by a 10 MHz, 12-bit ADC. The parallel processing of the signals permits a readout time of 22.5 μs per 64 pixels.

It is a particular feature of pn-CCDs that they allow to realize large pixels. For an optimal match to the angular resolution of the XMM telescope (≈20″) and to reduce readout time a pixel geometry of $150 \times 150\ \mu m^2$ has been chosen.

3. Performance parameter

Extended measurements have been performed at several X-ray test facilities of the Max-Planck-Institut für extraterrestrische Physik. The relevant results reflecting the state of the art of the single pn-CCD quality and our recent improvements are listed below.

3.1. Electronic and system noise, dark current

The equivalent noise charge of the pn-CCD detector system is $6\ e^-$ for an event integration time of 100 ms and a read out time of 4.5 ms. The noise shows neglegible temperature dependence between 120 and 190 K, reflecting

that dark current is small despite the deep depletion thickness. The recent improvements in the signal to noise ratio have been achieved by further reducing the anode stray capacitance. The largest noise contributions now arise from the CAMEX chip and from electronic pick-up.

3.2. Spatial uniformity

The spatial uniformity in the CCD performance is excellent. The recent fabrications yielded a large number of wafers with homogenous noise distribution and uniform spectroscopic behaviour. Only a small number of pixel defects (about one per chip) occurred. They are e.g. individual noisy pixels or a high charge transfer loss in a single pixel.

3.3. Space and time resolution

The spatial resolution is $43 \times 43\ \mu m^2$ if determined by the pixel size of $150 \times 150\ \mu m^2$. Due to the extent of the electron cloud of typically 20 μm it can even be improved for the so called split events, i.e. when two or more pixels share the charge generated by one X-ray photon.

In the full frame mode, which is the standard operating mode, an integration time of typically 100 ms is followed by a readout cycle of about 4.5 ms for the 200×64 pixels. However, a much higher time resolution can be achieved if the event integration is skipped in favour of a continuous readout. With the known position of a pulsed X-ray source it is possible to determine the time of arriving photons within 50 μs. To reduce the data rate 10 pixels are summed up before each amplification and readout of the 64 channels.

3.4. Energy resolution

Fig. 3 shows the energy resolution of the detector system as a function of the photon energy. The recent improvements are indicated as well as the final objective

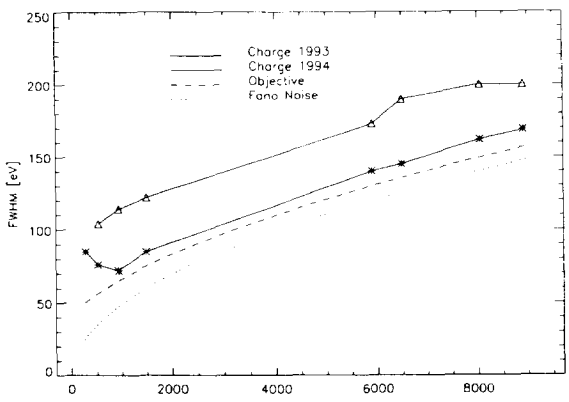

Fig. 3. Energy resolution of the pn-CCD versus X-ray energy.

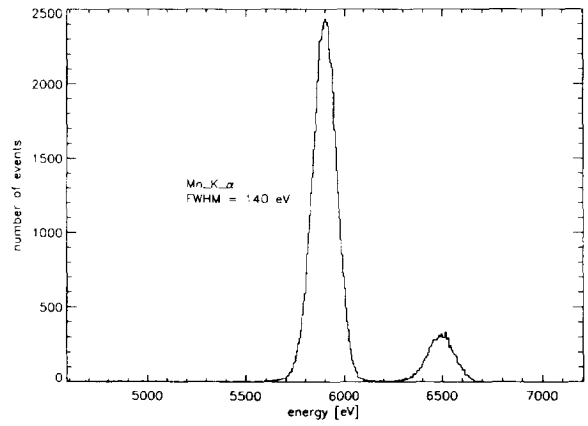

Fig. 4. ^{55}Fe spectrum ($T = 140$ K).

values for XMM. For low energies the energy resolution is determined by the electronic noise and the quality of the entrance window. At high energies the noise due to charge transfer inefficiency and the Fano noise, which sets the theoretical limit due to statistical fluctuations in the ionization process become dominant. As demonstrated in Fig. 3 the energy resolution is close to this physical limit. For illustration Fig. 4 shows a ^{55}Fe X-ray spectrum with 140 eV and 145 eV FWHM for the K_α and K_β lines respectively and Fig. 5 gives an aluminium spectrum with 85 eV FWHM. Fig. 9 shows a carbon spectrum with a FWHM of 85 eV (detection efficiency of 81%).

3.5. Charge transfer efficiency

The charge transfer efficiency of the pn-CCD is good and due to the number of only 200 transfers charge loss between the first and the last pixel is almost neglegible. For the scatter plot of signal height versus position in Fig. 6 the intensive radiation from a copper target in an X-ray

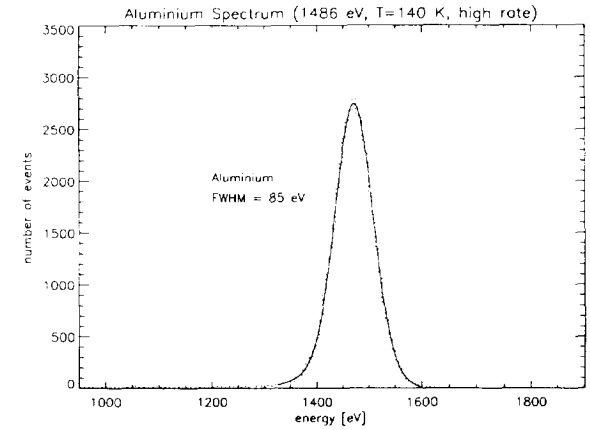

Fig. 5. Aluminium spectrum ($T = 140$ K).

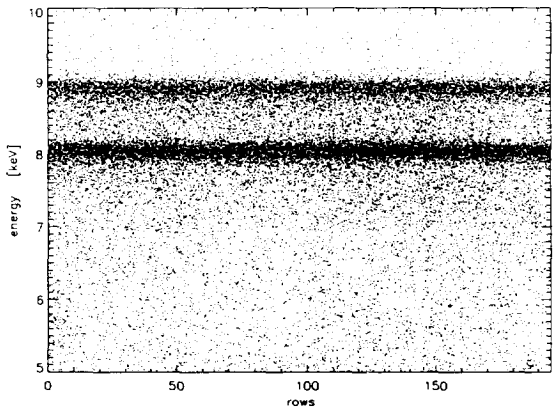

Fig. 6. Scatter plot: measured energy versus transfer length. The events were generated by intensive radiation from an X-ray tube using a copper target.

tube was used. The measurement was taken at 145 K, which is within the temperature range available on the satellite.

However, a certain dependence of the charge loss on temperature and signal rate is still observed as demonstrated in Fig. 7. The effect is dedicated to contaminations with energy levels at about 0.3 eV below the conduction band edge. The trap concentration is estimated by 10^{10} cm^{-3}. Different investigations have been started to identify and eliminate the trap levels, but final conclusions have not yet been drawn. A method, which uses the dependence of the charge transfer efficiency on temperature and operation parameters as an identification tool is presented in [4]. The most probable candidates are carbon related defects or titanium contaminations, brought into the material by the epitaxial process. To minimize the effect of the trap levels the design of the transfer channel and the operation parameters have been optimized, i.e. the electrons are collected and transferred within a 8 μm narrow region of the pixels. And, as mentioned before, readout time has been reduced to 4.5 ms.

3.6. Entrance window and quantum efficiency

The pn-CCD has the advantage to be illuminated from its unstructured side through a homogenous and thin entrance window. The quantum efficiency is high (better than 80%) over a wide energy range from 270 eV to 10 keV. Carbon photons e.g. with an X-ray energy of 277 eV are detected with an efficiency of 81% and an energy resolution of 85 eV FWHM is demonstrated in Figs. 8 and 9.

For low energy photons with small absorption length the quality of the entrance window is substantial. As the number of recombination centers is high very close to the detector surface, only a partial amount of the charge is collected in the transfer region. The resulting so called partial events reduce the quantum efficiency and the energy resolution of the detector. By performing the boron implantation of the entrance window diode through a silicon dioxide layer we were able to reduce the number of these events significantly. Further improvements are expected by additional modifications of the fabrication process.

For high energetic photons (>8 keV) a reduction of the quantum efficiency results from the increasing absorption length. However, due to the extended sensitive thickness of 280 μm the values are high compared to conventional CCDs.

Fig. 8 shows measurements of the detection efficiency in dependence of the X-ray energy. The continuous line between 70 eV and 3 keV represents DC-photocurrent measurements performed at the XS700 monochromator at the BESSY synchrotron [5]. The dotted line from 3 to 15 keV is the expected efficiency derived from the photon absorption data [6]. At six energies, i.e. for C, O, Cu_L, Si_K, Ti_K

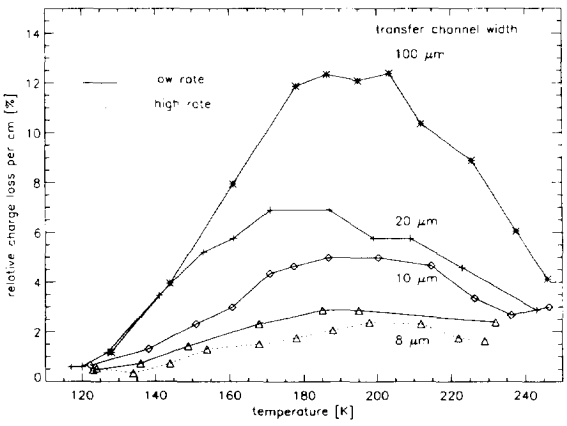

Fig. 7. The relative charge loss of the pn-CCD per 1 cm transfer length in dependence of the operating temperature and the intensity of an ^{55}Fe radioactive source.

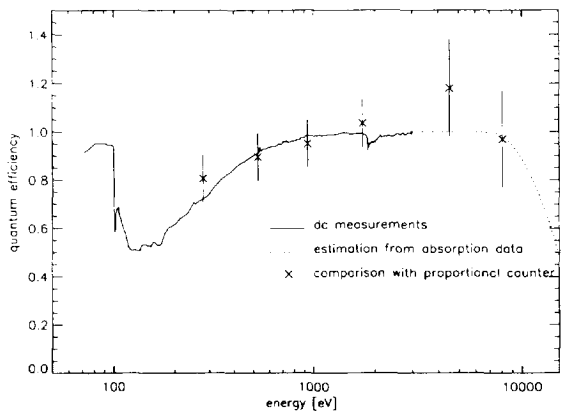

Fig. 8. Detection efficiency of the pn-CCD versus X-ray energy.

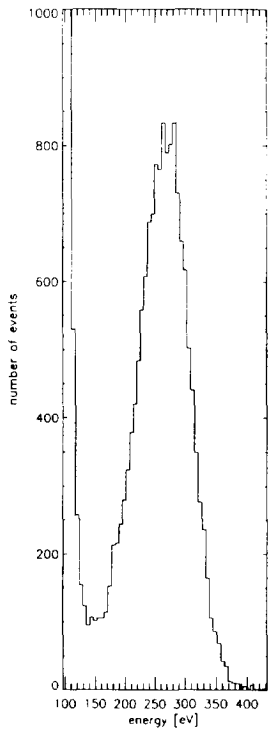

Fig. 9. Carbon spectrum ($T = 140$ K, FWHM = 85 eV).

and Cu_K, we measured the quantum efficiency in a single photon counting mode in comparison to the ROSAT position sensitive proportional counter PSPC [7]. The values are also included in the plot. The error bars are due to uncertainties of the PSPC measurements and the calibration of the experimental setup.

3.7. Charge splitting

The effect of charge splitting is much less pronounced in the pn-CCD as in conventional (MOS) CCDs due to the comparable large pixel size and the high drift field over the whole detection volume. A percentage of 75% of the photon events shows up as single events, only 2% split in three or four pixels. Summation of the split events is possible with good success.

3.8. Radiation hardness

The equivalent of the irradiation the CCDs will experience during the 10 year mission is a 3.5×10^8 cm^{-2} dose of 10 MeV protons. To simulate this and demonstrate the pn-CCDs radiation hardness they were exposed to 10 MeV protons from a tandem accelerator with doses up to 6.5×10^9 cm^{-2}. None of four irradiated and tested pn-CCDs failed after the irradiation. At the dedicated operating temperature of about 170 K the leakage current increase and degradation of the charge transfer efficiency are not significant. The reason is that the A-center defects, generated about 0.17 eV below the conduction band edge, lead to a maximum charge transfer loss at 120 K, but are not effective above 160 K.

As the transfer or the on-chip amplification of the signal electrons is not controlled by MOS structures it is unaffected by deteriorations of the gate oxide, in contrast to MOS-CCDs. The problem of radiation hardness is discussed in full detail in Ref. [4].

3.9. Background rejection

Minimum Ionizing Particles (MIPs) lose a certain amount of energy along their track. Taking into account the pixel size (150×150 μm^2), the CCD's sensitive thickness (280 μm) and arbitrary incidence angles of the MIPs an average 66 keV will be deposited in a single pixel. The probability to deposit more than 20 keV in at least one pixel of the track is larger than 0.99999 [8]. By these so-called bright pixels the particle track of a MIP is easily identified and separated from the X-ray photon events. Fig. 10 shows a representative MIP event with a small entrance angle. Beside few bright pixels (three for this event) the number of affected pixels in general is small. The on-board rejection analysis will identify the bright pixels and exclude them together with two surrounding "layers" of pixels to minimize the data rate.

4. Conclusion

The pn-CCD is a multi-purpose detector. The short cycle time permits the investigation of intensive X-ray sources; the high quantum efficiency guarantees satisfactory measurements of faint X-ray emitting objects.

The pixel size of 150×150 μm^2 has been adapted to the spatial resolution provided by the telescope. By parallel processing of the signals the read out time is reduced to 4.5 ms for a full frame, which corresponds to 0.35 μs per pixel. The time resolution varies between 50 μs (timing mode) and several tenth of ms (full frame mode).

The total electronic noise accounts to $6e^-$ ENC for operation temperatures between 120 K and 190 K (including noise sources from the detector and the readout system). The energy resolution reaches the physical limit given by Fano noise. An ^{55}Fe X-ray spectrum shows 140 eV FWHM. Due to a thin entrance window and a depletion thickness of 280 μm the quantum efficiency is larger than 80% over an energy range between 0.27 keV and 10 keV.

According to the above data almost all XMM requirements [9] have been achieved by the 1994 single chip fabrication of pn-CCDs. The first batch of 6×6 cm^2 devices was produced this year and is now tested. First measurement results of the electronic system noise indicate a noise level as low as 4.5 e^- between 120 K and 190 K.

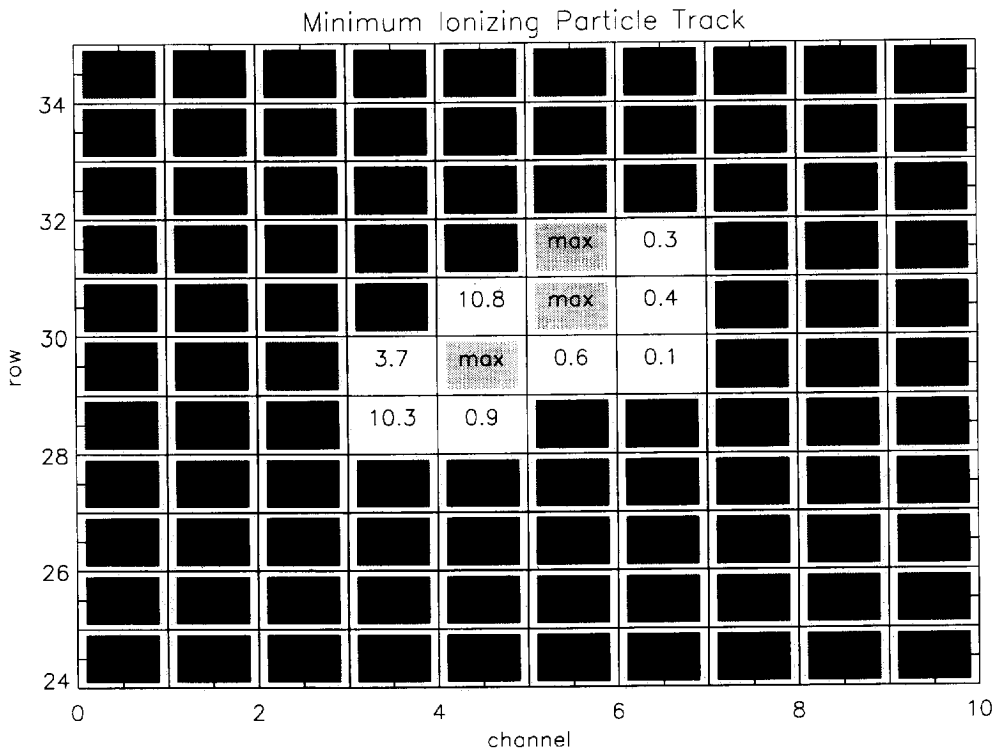

Fig. 10. Track of a minimum ionizing particle with a small entrance angle. Dark pixels are below threshold, numbers represent deposited energy in keV, "max" indicates signals above the ADC's dynamic range, i.e. >23 keV.

Preliminary investigations of the CCD entrance window have been performed demonstrating an improved low energy performance. Long term stability tests will also start this year.

References

[1] L. Strüder, H. Bräuninger et al., Nucl. Instr. and Meth. A 288 (1990) 227.
[2] H. Bräuninger, R. Danner et al., Nucl. Instr. and Meth. A 326 (1993) 129.
[3] W. Buttler, G. Lutz et al., Nucl. Instr. and Meth. A 288 (1989) 140.
[4] N. Meidinger, H. Soltau et al., Radiation hardness and defect analysis of an X-ray charge coupled device detector, Nucl. Instr. and Meth., to be published.
[5] H. Rabus, F. Scholze, R. Thornagel and G. Ulm, these Proceedings (7th Europ. Symp. on Semiconductor Detectors, Schloss Elmau, Bavaria, Germany, 1995) Nucl. Instr. and Meth. A 377 (1996) 209.
[6] B.L. Henke et al., Atom. Data Nucl. Data Tables 27 (1982) 1.
[7] E. Pfeffermann et al., SPIE 733 (1986) 519.
[8] R. Danner, Teilcheninduzierter Hintergrund bei Röntgensatelliten, Master's thesis, Technische Universität München, 1993.
[9] H. Bräuninger, E. Kendziorra et al., EPIC EOBB final report on the pn-EOBB tests, Technical report, MPE Garching, 1994.